DOI: https://doi.org/10.5592/CO/EUROENGEO.2024.178

APPLICATION OF MACHINE LEARNING FOR MODELLING SUBSURFACE SPATIAL MODEL USING GEOPHYSICAL AND BOREHOLE DATA – A CASE STUDY OF GUSIĆ POLJE 2 COMPENSATION BASIN FOR SENJ 2 HYDROELECTRIC POWER PLANT

MATIJA LOZIĆ[1], ANTONIA MIRČETA[2]

[1] *Elektroprojekt d.d., Croatia, matija.lozic@elektroprojekt.hr*

[2] *Elektroprojekt d.d., Croatia, antonia.mirceta@elektroprojekt.hr*

Abstract

Machine learning impacts everyday life in every field. This paper shows the application of machine learning in geoscience. Used machine learning model for classification and classification certainty estimation is ensembled from multilayer perceptrons each fitted in with different combination of variables. Used data consists of terrain data, borehole data, seismic refraction data and geoelectric data. Geophysics data was interpolated using IDW with a power parameter chosen based on a cross-validation process using mean squared error. Such prepared data was preprocessed and 49 data subsets were defined. Each multilayer perceptron was fitted in with the corresponding data subset using an optimal hyperparameter for that model. For ensemble learning classification max voting was used. Using a ratio of max voted class and number of votes certainty classification was estimated. Basic model metrics and prediction results are shown. Predictions are used for calculating robust orientational settlement map.

Keywords

Machine learning, Ensemble learning, Multilayer perceptron, Geostatistics, Inverse distance weighting (IDW), Modified Shepard's method, Geotechnical investigation, Subsurface spatial model, Gusić polje, Hydropower System Senj 2, settlement estimation.

1 Introduction

Geostatistics is a standard tool in geology used for analyzing and visualizing various types of data. It allows for the effective analysis of spatial variability and the creation of geological models.

By integrating multiple data sources such as boreholes, geophysical profiles, and remote sensing data, geostatistics provides a robust framework for subsurface characterization and natural hazard assessment. Techniques like kriging and inverse distance weighting are commonly used to interpolate and predict spatial models.

Pioneers of geostatistics in geology include Georges Matheron and Michel David. Georges Matheron is considered the founder of geostatistics, having developed the theoretical foundations and coined the term in the early 1960s. Michel David further advanced the field with his work on practical applications, particularly in mining geology. Their contributions have laid the groundwork for modern geostatistical methods used widely in geological and environmental studies.

This paper examines geostatistical methods combining machine learning to generate a subsurface spatial model. The main objectives of this study are to (1) provide a subsurface a spatial model (2) provide spatial certainty model and (3) create a settlement map of foundation soil after the construction water load.

Figure 1. The broader project area showing the existing Gusić polje basin and the designed Gusić polje 2 basin

The study area is located in central Croatia, in Ličko-Senjska County. The Senj Hydropower System (HPS) utilizes the water potential of the Lika and Gacka Rivers, situated between the Lička Visoravan plateau and the Adriatic Sea.
The Lika River, with a catchment area of approximately 1125 km² and an average annual flow rate of about 28.76 m³/s, is a torrential stream with flow rates ranging from 0 to 1300 m³/s. The Gacka River has a catchment area of 584 km² and an average annual flow rate of about 15.65 m³/s, with flow rates ranging from 3.5 m³/s to 149 m³/s.
The Senj HPS diverts water from the Lika River into the Gacka River and channels it through a common system for power generation in the Senj Hydroelectric Power Plant (HPP) with a maximum gross head of 437 meters. To reduce spillage losses, the second stage, HPP Senj 2, has been planned. The HPP Senj 2 project includes the construction of the Gusić Polje 2 Compensation Basin, featuring 3,664.06 meters of lateral embankments and a storage capacity of 2.87 million cubic meters for daily inflow regulation. The basin and embankments will be waterproofed using geomembrane techniques.
The existing Gusić Polje Compensation Basin of HPS Senj lies on the natural ground with karstic phenomena and is lined with clay. The new compensation basin, Gusić Polje 2, will be constructed adjacent to the existing one, connected via a culvert. Due to geological characteristics, settlements are expected. The surfaces to be covered include the slopes and bottom of the existing reservoir.
For this technical solution, calculating the settlements of the basin and embankments' foundation soil is essential. Various geotechnical investigations, geophysics, and exploratory boreholes have been conducted in the area over the years. Estimating the spatial distribution and thickness of strata in karst landscapes is challenging, requiring advanced estimation techniques.
Section 2 shows used raw data from geotechnical site investigations and terrain data. Section 3 presents data preprocessing. Sections 4 and 5 present model creation and evaluation by basic classification metrics. Section 6 is the results of predictions and section 7 is settlement calculations. Further in section 8 is an interpretation of results and section 9 discussion.

2. Raw data

Raw data used in this paper are terrain data, boreholes data, geoelectric tomography data and seismic refraction data.
For project purposes terrain survey was conducted and a TIN model was built. Raw terrain data is a collection of TIN points on the grid. Grid parameters of collected points are shown below in Table 1.

The grid raster from which data was collected is raster used all along in this paper.

Table 1. Spatial variables boundary and step values

	min	max	step
x - Easting	390320	391500	10
y - Northing	4978340	4979420	10
z - Elevation	410.1	456.7	0.2
d - Depth	0	20	0.2

Borehole data was collected during site investigations. Drilling was performed in both soil and carbonate rock. During drilling in cohesive soil, undisturbed samples were taken, and a standard penetration test (SPT) was conducted approximately every 2 meters. Extracted cores were placed in labeled core boxes and photographed. They were then mapped by a geologist, who also conducted approximate uniaxial strength tests using a manual penetrometer. Characteristic soil and rock samples were selected for geotechnical laboratory testing. The groundwater level was measured and recorded post-drilling.
In all 92 boreholes were drilled. They essentially detected three materials: tuff, clay and limestone. To limestone material weathered zones were added.
Three types of stratigraphy can be concluded from core drillings. Stratigraphy one is when tuff is above clay and clay is above limestone, second stratigraphy is the absence of clay in the middle, and third stratigraphy is the absence of tuff on the surface.
Geoelectrical tomography was conducted to determine the depth and thickness of sediments in alluvial deposits, identifying lateral contacts in the underlying soil or rock due to lithological changes, creating vertical sections of materials and rocks along specified profiles, and locating fault zones.
A total of 9440 meters of geoelectrical tomography was performed across 16 profiles at the Gusić Polje 2 site using Wenner's electrode arrangement, with spacings of 2 and 5 meters. This setup provided interpretation depths of 24-60 meters. The profile locations matched those of the boreholes.
The results of the geoelectrical test are presented in a multicolored two-dimensional section of the deposit resistivity distribution (Table 2). The presentation also contains prognostic lithological determination based on resistance, geological mapping and core determination of boreholes in the research areas.

Table 2. Prognostic Lithological Determination Based on Geoelectrical Tomography Results

Resistance (Ωm)	Material
0 to 45	Clay, dust, fine rubble
45 to 100	Mixture of rubble, clay, and sands
100 to 600	Highly to moderately fragmented carbonate rock mass, cracks mostly filled with rubble and clay
600 to 7000	Poorly fragmented to compact carbonate rock mass, with fault zones possibly containing minor cracks and caverns
> 7000	Zone of possible cracks without filling, minor caverns

Geophysical investigations conducted in 1997 aimed to differentiate rock cover deposits in the subsoil using refraction seismic. Twenty-one profiles were surveyed with 135 geophones set along each profile and three shots per device. This geophone configuration enabled research to a depth of up to 40 meters. The refraction seismics identified four elastic environments based on primary elastic wave velocities:

1. Surface Complex: Velocities < 500 m/s, including various sediments and materials.
2. Cover Deposits: Velocities 600-1600 m/s, consisting of clays, weathered rock, and cavernous limestone.
3. Fractured Rock: Velocities 1480-2300 m/s, comprising fractured rock and zones of weaker rock.
4. Compact Rock: Velocities 2100-4000 m/s, including moderately fractured to compact rock.
5.

3. Data preprocessing

The terrain data presented in Section 2 are discretized by depth at every 0.2 meters. At each point, a new elevation is calculated by subtracting the terrain surface elevation by depth, resulting in a data format as *{x, y, z, d}*. Borehole data, also presented in Section 2, are discretized by depth at every 0.2 meters, collecting the material in the corresponding interval. This data collection continues to a depth of 20 meters for each borehole. After processing, each discretized point contains variables *{x, y, z, d, and material}*. The material is encoded with integers as follows: Tuff – 1, Clay – 2, and Limestone – 3.
Geophysics data was spatially interpolated using Inverse Distance Weighting (IDW). IDW Power parameter was chosen based on a cross-validation process in a 70/30 ratio, observing mean absolute error and mean squared error of residuals between estimated and true values. Chosen power parameters were parameters obtained from averaging power parameters that produce a minimum of MAE and MSE functions. Interpolation was applied first on profile data and then on depth planes every 0.2 m on terrain data grid points and borehole data points.
Seismic refraction profiles interpolation was the exception, instead, IDW Modified Shepard's method was used, due to unfavorable data locations. A radius of influence of 35m was chosen. 35 m was a minimal value where data loss was acceptable. The cross-validation process of power parameter for IDW interpolation of seismic refraction depth planes data shows which is a good average power parameter. After the cross-validation process of the power parameter for IDW interpolation of geoelectric tomography profile data chosen power parameter was 3, and for depth planes was 5.
After the interpolation process in each point on the grid data takes form *{x, y, z, d, v, ohmm}*, the exception is borehole data which points have form *{x, y, z, d, v, ohmm, material code}*. From such formed data 49 data subsets were defined, each subset containing a different combination of variables.
The data was normalized to values between 0 and 1 using a simple min-max scaler. The minimum and maximum values were selected from the entire data domain. To define the training and testing datasets for model fitting, the boreholes were split into training and testing sets in a 70/30 ratio. The resulting train and test datasets had imbalanced classes. To address this, data containing dominant classes were removed until a class balance was achieved and applied to both the training and testing datasets.

4. Multilayer perceptron

As weak learners multilayer perceptron for classification (MLPC) was chosen. MLPC is classified as supervised machine learning feedforward model, detailed description can be found in Gareth(2023). Model architecture is defined by its hyperparameters.
In this paper on each data subset different MLPC is used, with its own hyperparameters that are chosen by searching hyperparameter grid space observing accuracy on train set. Hyperparameters that was searched are: hidden layer size, activation function, l2.- regularization coefficient, Discrete value of each hyperparameter is presented in Table 3. To mitigated overfitting early stopping is used. As activation function of output layer softmax function is used. Output layer consists of three neurons, one for each class.

Table 3. Discrete values of multilayer perceptron hyperparameters

Number of hidden layers	form 1 to 3
Number of neurons in hidden layer	from 2 to 10
Activation function	['relu', 'tanh']
l2-regularization coefficient	[0.00001, 0.0001, 0.001, 0.01, 0.1]

Each MLPC model is fitted on train data using "optimal" hyperparameters and tested on test data.
Basic metrics are conducted on train and test data to show how good a certain model is. Basic metrics contain for train dataset and test dataset accuracy, precision for each class, recall for each class and f1-score for each class.
Accuracy measures how many certain class is classified correctly. Expression for calculating accuracy:

$$Accuracy = \frac{(TP+TN)}{(TP+TN+FP+FN)} \quad (1)$$

Precision measures how many predictions as certain class is actual class. Precision is calculated by expression:

$$Precision = \frac{TP}{(TP+FP)} \quad (2)$$

Recall measures how many model correctly classified certain class compared to actual existing class in dataset

$$Recall = \frac{TP}{(TP+FN)} \quad (3)$$

F1-score is harmonic mean of precision and recall. F1-score measures how well model balances between precision and recall.

$$F1score = 2 \cdot \frac{Precision \cdot Recall}{Precision+Recall} \quad (4)$$

where:
TP – Number of true positives [1]
TN – Number of true negatives [1]
FP – Number of false positives [1]
FN – Number of false negatives [1]

Basic metrics of individual MLPCs for train and test data are shown in Table 4, also data subset parameters are introduced. Models on average had accuracy little below 70% on train and test data. The small difference between test and train accuracy indicates that there is no overfitting. For limestone class metrics show good performances, for tuff class fairly good, but for clay class metrics indicate poor performance, especially recall and consequently F1 score. This can be due to thick transitional zones of tuff and clay, weathered limestone discontinuities filled with clay and other reasons.

5. Model ensemble

To achieve a more robust estimator, model ensembling was employed, as detailed in Chollet (2017). The ensemble in this paper consists of 49 multilayer perceptron models from Section 4. The ensemble method used for the final classification was max voting, meaning the final classified class is the one with the most votes from all models.
The introduced model ensemble is also used for creating a certainty map according to (5) which can be found in Erharter(2021) that helps visualize which area of the site is less certain and prone to additional investigation. Additionally, certainty is used for determining and displaying material noisy boundaries and geological features, such as faults and weathering zones.

$$c = \frac{\left\{max\left(\frac{\sum_1^n \hat{y}}{n}\right) - \frac{1}{n_{classes}}\right\}}{1 - \frac{1}{n_{classes}}} \quad (5)$$

where:
c– certainty
$\hat{y}$ – class classified from single weak learner
n – number of weak learners
$n_{classes}$ – number of classes

Table 4. Basic metrics on train and test data of multilayer perceptrons

Model	Data Subset parameters	TRAIN										TEST									
		Acc	Class 1 - Tuff			Class 2 - Clay			Class 3 - Limestone			Acc	Class 1 - Tuff			Class 2 - Clay			Class 3 - Limestone		
			P	R	F1	P	R	F1	P	R	F1		P	R	F1	P	R	F1	P	R	F1
1	v, ohmm	0.68	0.71	0.54	0.62	0.52	0.59	0.55	0.81	0.90	0.85	0.66	0.72	0.52	0.60	0.53	0.63	0.57	0.78	0.85	0.81
2	x, v	0.68	0.68	0.81	0.74	0.62	0.26	0.37	0.69	0.95	0.80	0.64	0.72	0.74	0.73	0.52	0.28	0.37	0.62	0.90	0.73
3	x, ohmm	0.46	0.43	0.68	0.53	0.90	0.06	0.11	0.46	0.62	0.53	0.41	0.51	0.48	0.49	0.39	0.11	0.18	0.37	0.66	0.47
4	x, v, ohmm	0.72	0.67	0.81	0.74	0.64	0.43	0.51	0.80	0.90	0.85	0.67	0.71	0.75	0.73	0.55	0.43	0.49	0.72	0.85	0.78
5	y, v	0.66	0.65	0.75	0.70	0.60	0.32	0.42	0.70	0.91	0.79	0.66	0.62	0.84	0.71	0.56	0.30	0.39	0.76	0.84	0.80
6	y, ohmm	0.45	0.37	0.82	0.51	0.47	0.25	0.33	1.00	0.27	0.43	0.42	0.37	0.91	0.52	0.45	0.13	0.20	1.00	0.22	0.36
7	y, v, ohmm	0.63	0.59	0.66	0.62	0.53	0.30	0.38	0.70	0.91	0.79	0.59	0.52	0.80	0.63	0.38	0.15	0.21	0.78	0.86	0.81
8	z, v	0.65	0.58	0.92	0.71	0.49	0.30	0.37	0.89	0.73	0.80	0.65	0.58	0.91	0.71	0.49	0.31	0.38	0.91	0.74	0.82
9	z, ohmm	0.66	0.60	0.95	0.73	0.62	0.27	0.37	0.79	0.78	0.79	0.71	0.62	0.96	0.75	0.73	0.34	0.47	0.84	0.83	0.84
10	z, v, ohmm	0.63	0.58	0.89	0.70	0.37	0.10	0.15	0.74	0.88	0.81	0.66	0.59	0.88	0.70	0.58	0.20	0.30	0.80	0.93	0.86
11	d, v	0.73	0.69	0.85	0.76	0.62	0.48	0.54	0.85	0.86	0.85	0.76	0.69	0.87	0.77	0.67	0.57	0.62	0.94	0.83	0.88
12	d, ohmm	0.75	0.71	0.83	0.76	0.64	0.58	0.61	0.90	0.85	0.87	0.77	0.72	0.84	0.78	0.67	0.67	0.67	0.97	0.81	0.88
13	d, v, ohmm	0.70	0.75	0.69	0.72	0.55	0.51	0.53	0.77	0.89	0.83	0.76	0.80	0.66	0.73	0.65	0.69	0.67	0.84	0.94	0.88
14	x, y, v	0.63	0.61	0.84	0.71	0.51	0.16	0.25	0.68	0.89	0.77	0.63	0.67	0.83	0.74	0.51	0.28	0.36	0.65	0.81	0.72
15	x, y, ohmm	0.47	0.43	0.66	0.52	0.59	0.13	0.21	0.49	0.62	0.55	0.44	0.47	0.71	0.57	0.38	0.03	0.05	0.40	0.59	0.48
16	x, y, v, ohmm	0.72	0.70	0.72	0.71	0.60	0.53	0.56	0.84	0.90	0.87	0.71	0.72	0.75	0.74	0.60	0.54	0.57	0.79	0.84	0.81
17	x, z, v	0.70	0.62	0.92	0.74	0.66	0.26	0.38	0.80	0.90	0.85	0.72	0.66	0.88	0.75	0.72	0.36	0.48	0.80	0.94	0.86
18	x, z, ohmm	0.54	0.50	0.76	0.61	0.31	0.15	0.20	0.69	0.70	0.69	0.59	0.66	0.67	0.67	0.50	0.35	0.41	0.58	0.76	0.66
19	x, z, v, ohmm	0.73	0.67	0.86	0.75	0.71	0.39	0.50	0.79	0.92	0.85	0.69	0.71	0.82	0.76	0.61	0.39	0.48	0.72	0.89	0.80
20	x, d, v	0.75	0.73	0.74	0.74	0.64	0.56	0.60	0.85	0.93	0.89	0.74	0.82	0.62	0.70	0.61	0.70	0.65	0.84	0.92	0.88
21	x, d, ohmm	0.75	0.81	0.68	0.74	0.59	0.76	0.66	0.90	0.80	0.85	0.78	0.89	0.71	0.79	0.63	0.84	0.72	0.91	0.79	0.85
22	x, d, v, ohmm	0.76	0.66	0.92	0.77	0.72	0.45	0.56	0.92	0.89	0.90	0.78	0.73	0.94	0.82	0.75	0.57	0.65	0.90	0.85	0.87
23	y, z, v	0.66	0.63	0.82	0.71	0.54	0.24	0.34	0.73	0.90	0.81	0.73	0.65	0.91	0.76	0.80	0.32	0.46	0.79	0.96	0.87
24	y, z, ohmm	0.57	0.48	0.75	0.59	0.52	0.30	0.38	0.76	0.65	0.70	0.53	0.43	0.89	0.58	0.55	0.15	0.24	0.89	0.57	0.69
25	y, z, v, ohmm	0.66	0.61	0.81	0.70	0.54	0.26	0.35	0.77	0.91	0.83	0.69	0.61	0.90	0.72	0.62	0.31	0.41	0.85	0.87	0.86
26	y, d, v	0.64	0.88	0.34	0.49	0.48	0.71	0.57	0.77	0.87	0.82	0.69	0.88	0.34	0.50	0.53	0.90	0.67	0.92	0.83	0.87
27	y, d, ohmm	0.73	0.74	0.80	0.77	0.59	0.60	0.60	0.87	0.78	0.82	0.74	0.74	0.81	0.77	0.60	0.71	0.65	0.97	0.69	0.80
28	y, d, v, ohmm	0.67	0.56	0.98	0.71	0.61	0.30	0.41	0.93	0.72	0.81	0.61	0.52	0.97	0.68	0.50	0.23	0.32	0.99	0.65	0.78
29	z, d, v	0.68	0.71	0.75	0.73	0.57	0.35	0.44	0.70	0.92	0.79	0.69	0.71	0.66	0.68	0.60	0.43	0.50	0.73	0.99	0.84
30	z, d, ohmm	0.73	0.72	0.78	0.75	0.60	0.54	0.57	0.84	0.86	0.85	0.77	0.74	0.78	0.76	0.66	0.69	0.67	0.94	0.84	0.89
31	z, d, v, ohmm	0.69	0.58	0.96	0.72	0.65	0.31	0.42	0.89	0.78	0.83	0.68	0.57	0.97	0.72	0.63	0.33	0.43	0.96	0.75	0.84
32	x, y, z, v	0.68	0.76	0.55	0.64	0.54	0.57	0.56	0.74	0.90	0.81	0.63	0.82	0.50	0.62	0.49	0.57	0.53	0.68	0.83	0.75
33	x, y, z, ohmm	0.51	0.86	0.40	0.55	0.42	0.26	0.32	0.45	0.85	0.59	0.52	0.89	0.47	0.62	0.53	0.16	0.25	0.42	0.95	0.59
34	x, y, z, v, ohmm	0.71	0.68	0.75	0.71	0.60	0.45	0.51	0.81	0.92	0.86	0.73	0.72	0.81	0.76	0.66	0.52	0.58	0.79	0.86	0.83
35	x, y, d, v	0.76	0.73	0.80	0.76	0.67	0.58	0.62	0.88	0.91	0.90	0.79	0.75	0.90	0.82	0.73	0.61	0.67	0.89	0.86	0.87
36	x, y, d, ohmm	0.70	0.65	0.82	0.73	0.66	0.36	0.47	0.78	0.92	0.84	0.73	0.68	0.93	0.79	0.81	0.41	0.54	0.77	0.87	0.82
37	x, y, d, v, ohmm	0.77	0.76	0.78	0.77	0.66	0.62	0.64	0.88	0.90	0.89	0.83	0.83	0.88	0.85	0.76	0.74	0.75	0.92	0.88	0.90
38	x, z, d, v	0.73	0.63	0.95	0.76	0.76	0.30	0.43	0.84	0.92	0.88	0.72	0.66	0.95	0.78	0.80	0.31	0.45	0.78	0.92	0.84
39	x, z, d, ohmm	0.74	0.71	0.80	0.75	0.66	0.48	0.56	0.81	0.92	0.86	0.74	0.83	0.82	0.82	0.67	0.52	0.59	0.72	0.90	0.80
40	x, z, d, v, ohmm	0.71	0.68	0.79	0.73	0.63	0.38	0.47	0.78	0.96	0.86	0.66	0.66	0.75	0.70	0.53	0.29	0.38	0.72	0.97	0.83
41	y, z, d, v	0.71	0.65	0.92	0.76	0.68	0.29	0.41	0.79	0.91	0.85	0.75	0.63	0.96	0.76	0.77	0.40	0.52	0.92	0.90	0.91
42	y, z, d, ohmm	0.70	0.68	0.83	0.75	0.60	0.40	0.48	0.79	0.88	0.83	0.70	0.59	0.91	0.72	0.65	0.31	0.43	0.91	0.89	0.90
43	y, z, d, v, ohmm	0.73	0.68	0.90	0.78	0.67	0.40	0.50	0.82	0.88	0.85	0.75	0.64	0.94	0.76	0.72	0.43	0.54	0.94	0.87	0.91
44	x, y, z	0.50	0.51	0.60	0.55	0.43	0.28	0.34	0.53	0.61	0.56	0.45	0.53	0.53	0.53	0.35	0.29	0.32	0.46	0.53	0.49
45	x, y, d	0.76	0.70	0.87	0.77	0.69	0.50	0.58	0.88	0.90	0.89	0.81	0.77	0.93	0.85	0.79	0.63	0.70	0.88	0.89	0.89
46	x, y, z, d	0.75	0.73	0.83	0.77	0.65	0.55	0.60	0.86	0.88	0.87	0.80	0.72	0.91	0.80	0.76	0.62	0.68	0.97	0.87	0.92
47	x, y, z, d, v	0.76	0.77	0.78	0.78	0.66	0.58	0.62	0.84	0.92	0.88	0.84	0.83	0.88	0.86	0.79	0.70	0.74	0.88	0.93	0.90
48	x, y, z, d, ohmm	0.77	0.77	0.78	0.78	0.65	0.62	0.64	0.86	0.89	0.88	0.87	0.88	0.89	0.89	0.80	0.83	0.81	0.94	0.89	0.91
49	x, y, z, d, v, ohmm	0.76	0.72	0.84	0.78	0.68	0.52	0.59	0.86	0.90	0.88	0.74	0.66	0.92	0.77	0.70	0.43	0.54	0.89	0.88	0.88
Min		0.45	0.37	0.34	0.49	0.31	0.06	0.11	0.45	0.27	0.43	0.41	0.37	0.34	0.49	0.35	0.03	0.05	0.37	0.22	0.36
Mean		0.68	0.66	0.78	0.70	0.60	0.40	0.46	0.79	0.84	0.81	0.69	0.68	0.80	0.72	0.62	0.44	0.49	0.80	0.83	0.80
Max		0.77	0.88	0.98	0.78	0.90	0.76	0.66	1.00	0.96	0.90	0.87	0.89	0.97	0.89	0.81	0.90	0.81	1.00	0.99	0.00

Figure 2 shows the confusion matrix of the model ensemble, the matrix indicates good ensemble performance on tuff and limestone classes, but clay class remains problematic.

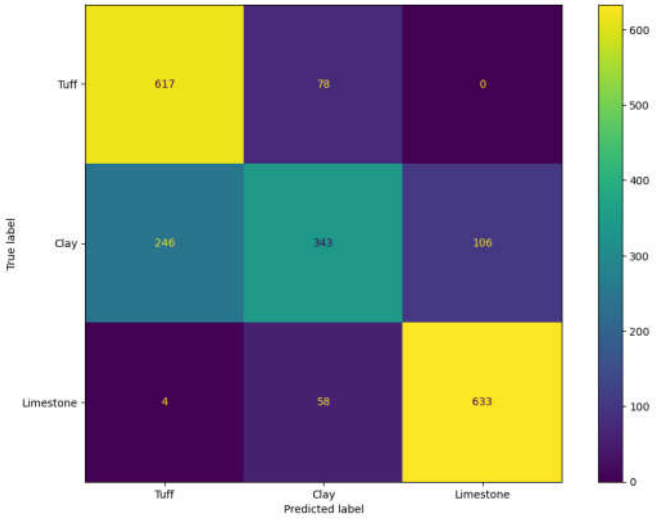

Figure 2. Confusion matrix of model ensemble prediction on all data

Table 5. Basic metrics of model ensemble

	Precsion	Recall	f1-score
Tuff	0.71	0.89	0.79
Clay	0.72	0.49	0.58
Limestone	0.86	0.91	0.88
Ensembe accuracy	0.76		

The model ensemble improved all average metrics from Table 5 by 3% to 12%. The most notable increase was observed in the clay class, which initially had the poorest metrics from individual classifiers, as well as in the overall ensemble classification. This indcates the usfullness of the ensemble method.

6 Results

The model ensemble for classification developed in the previous section was applied to the preprocessed input data. Below, we present some prediction results as examples of what can be generated from such a model.

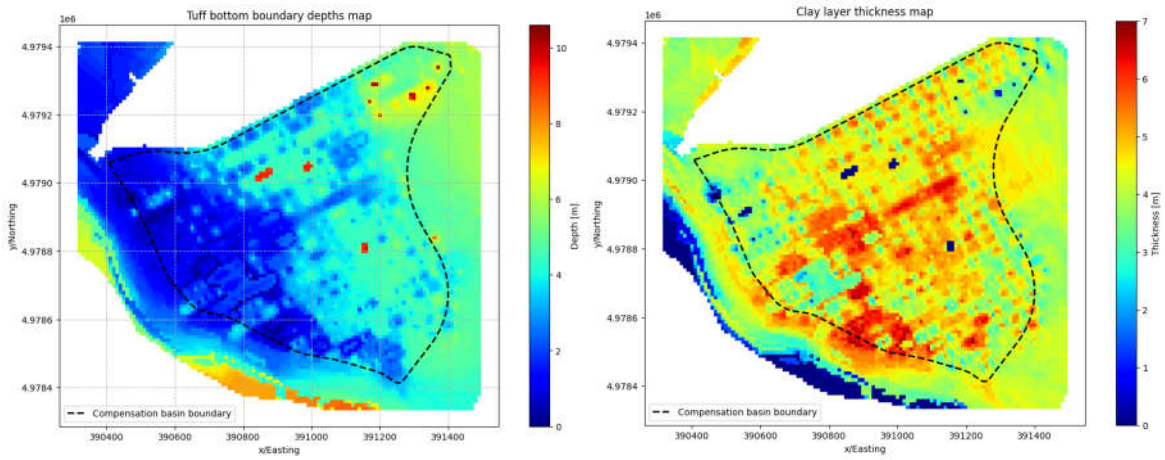

Figure 3. (left) Tuff layer bottom boundary map, (right) Clay layer thickness map

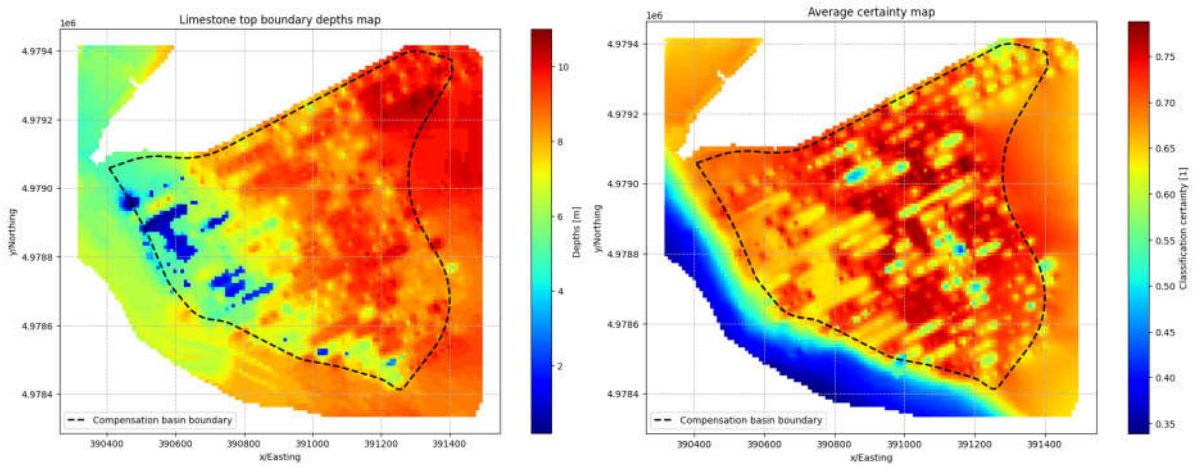

Figure 4. (left) Limestone surface depths, (right) Generated average certainty map

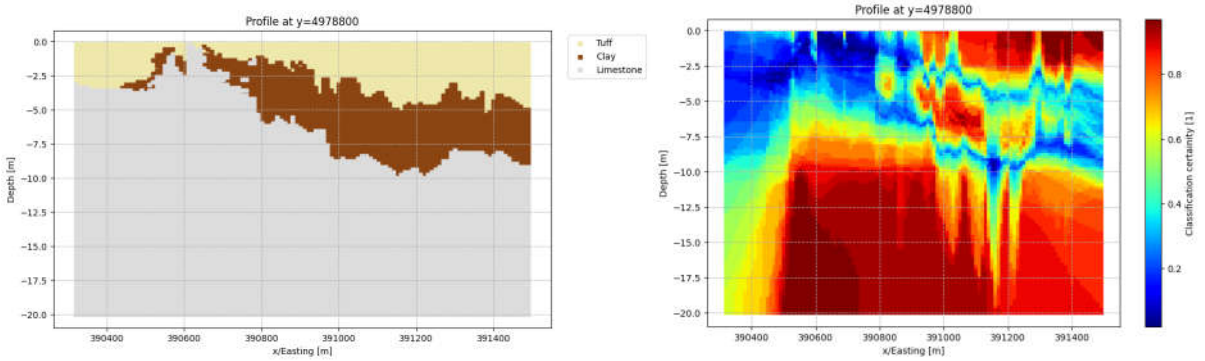

Figure 5. (left) Classification result profile at y= 4978800 on x-d plane , (right) Classification certainty profile at y= 4978800 on x-d plane

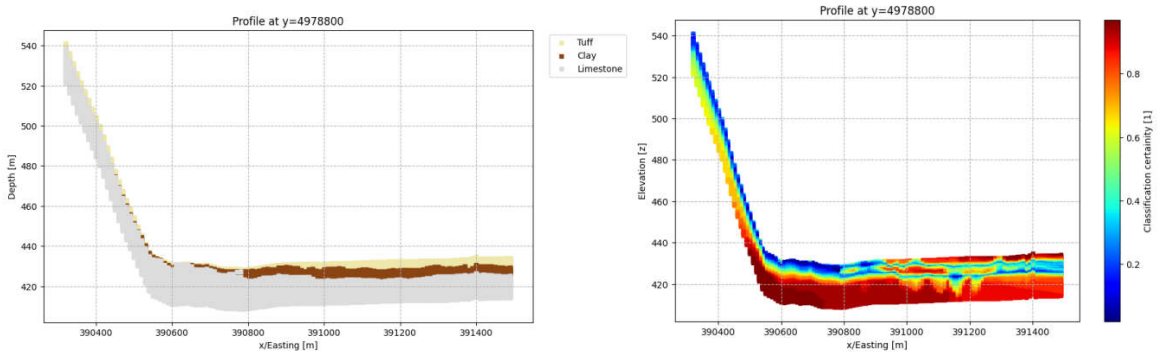

Figure 6. (left) Classification result profile at y= 4978800 on x-z plane, (right) Classification certainty profile at y= 4978800 on x-z plane

7 Settlement

A Settlement was calculated using the formula for soil deposits under a uniform load of the future hydrostatic pressure to 48kPa which is equivalent of 4.8m water column. Total settlement is the sum of deformations of individual soil layers, determined by stress changes and compressibility. The soil column is divided into layers with assumed uniform compressibility. Calculated settlement has an orientational purpose, just to show which area is more prone to settlement.

The expression for calculating the settlement is as follows:

$$s = \frac{\sigma}{E_s} H \tag{6}$$

where:
s- soil settlement,
σ- vertical load,
H- height of the soil layer,
E_s- oedometer modulus of deformation.

As previously mentioned, the subsurface spatial model was generated using data points on a 10 x 10 m grid. During the settlement map generation, each layer at each point was assigned a deformation modulus based on whether it was tuff or clay which is given below. The settlement for each layer at each point was calculated and summed to give the total settlement and the settlement map was created as shown in Figure 7.
Used oedometer modulus of soil deposits: Tuff - $E_s = 2\ MPa$ and Clay - $E_s = 10\ MPa$

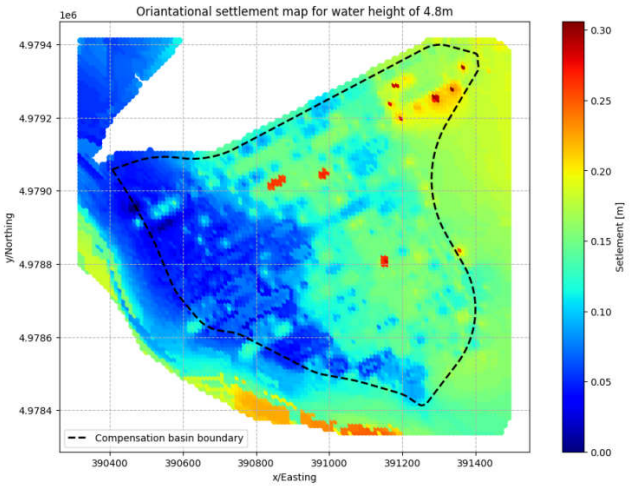

Figure 7. Settlement map

8 Interpretation of results

The results of this work include a spatial subsurface model, a spatial classification certainty model, and a settlement map, with this paper presenting only a glimpse of the findings. The aim is to demonstrate the value of the output from such models. In Figure 3(left), three areas with thick tuff deposits are observed, with tuff thickness increasing in the northeast direction, as does the clay, as shown in Figure 3(right). A limestone bedrock ridge is detected in the same direction, dividing the basin into two parts, as confirmed by the profile in Figures 5 and 6. The most intriguing aspect is the classification certainty of the profiles. At material boundaries, the certainty is almost 0, which is expected. However, the interesting parts are the low certainty zones in the limestone, which can be interpreted as fault zones or extremely weathered rock, essentially mixed limestone boulders with clay. These zones were added to the limestone as mentioned in Section 2. The average certainty map of the site highlights locations with low average certainty that are prone to additional investigations. Nevertheless, below the limestone layer, which has high certainty at bedrock locations, this high certainty significantly impacts the average values. The settlement map shows a resemblance to the tuff boundary depths map. This similarity is reasonable because tuff has five times more influence on settlement than clay.

9 Conclusion

This paper demonstrates the implementation of geostatistics and machine learning in geosciences for creating spatial subsurface models. Machine learning has an advantage over classical interpolation methods because it is better in generalization and can effectively deal with large high-dimensional, large datasets, can solve highly non-linear problems, and its computational complexity results are lower. After

preprocessing the raw data, multilayer perceptrons were fitted to different data subsets. While the overall metrics of the individual multilayer perceptron models were slightly above chance, combining them with the ensemble method resulted in a powerful and robust tool. The results presented in this paper highlight various applications of such a model. A spatial subsurface model was created, an average certainty map was generated, and information about soil deposits and the limestone surface was derived. Additionally, geomorphological features can be detected, although such claims require further validation. However, the model has its limitations. While it generalizes well, some specific information is lost. For instance, the model could not detect areas where tuff is directly above limestone or where clay is on the terrain surface, and it has a problem with correctly classifying clay. Nonetheless, these areas exhibit low certainty, demonstrating the effectiveness of the classification certainty model.

References

HE Senj 2, *Dno bazena i popratni nasipi, Geotehnički istražni radovi za izradu glavnog projekta, Elaborat za dno bazena i popratne nasipe*, INSTITUT IGH d.d., Zavod za projektiranje, Odjel za geotehnička istraživanja, Janka Rakuše 1, 10 000 Zagreb, Zagreb, veljača 2023.

HE Senj 2 – Glavni projekt, Kompezacijski bazen Gusić polje 2, Geološki radovi, Institut za geološka istraživanja – Zagreb, Sachsova 2, Zavod za hidrogeologiju i inženjersku geologiju, Zagreb, veljača 1998.

Kompezacijski bazen Gusić polje 2, Geofizička istraživanja, Moho d.o.o., Zagreb, svibanj 1997.,

HEP d.d. (Hrvatska elektroprivreda d.d.). Available online: www.hep.hr/projekti/hidroenergetski-sustav-senj-2/247 (accessed on 11 July 2024).

Chollet, F. (2017). *Deep learning with python*

Erharter, G. H., Oberhollenzer, S., Fankhauser, A., Marte, R., & Marcher, T. (Year). *Learning decision boundaries for cone penetration test classification.* Institute of Rock Mechanics and Tunnelling, Graz University of Technology, Graz, Styria, Austria; Institute of Soil Mechanics, Foundation Engineering and Computational Geotechnics, Graz University of Technology, Graz, Styria, Austria. Correspondence to G. H. Erharter (erharter@tugraz.at)

Garet, J. et al. (2023), *An Introduction to Statistical Learning* – with Applications in Python

Isaaks, E. H., & Srivastava, R. M. (1989). *Applied Geostatistics.* New York: Oxford University Press.

Davis, J. C. (2002). *Statistics and Data Analysis in Geology* (3rd ed.). Hoboken, NJ: Wiley.

Sever Z., *Hydroelectric power plants in Croatia*, Hrvatska elektroprivreda d.d., Elektrprojekt Consulting Engineers, Zagreb, February 2000.